Journal of the European Ceramic Society **14** (1994) 313–325

Thermal Behavior of Polymer-Derived Ceramics. IV. Si–C–N–O Fibers from an Oxygen-Cured Polycarbosilazane

O. Delverdier, M. Monthioux

Laboratoire Marcel Mathieu, CNRS-UPPA, Centre Hélioparc, 2 av. Du Président P. Angot, F64000 Pau, France

D. Mocaer & R. Pailler

Laboratoire des Composites Thermostructuraux, UMR 47 CNRS-SEP-UB1, Domaine Universitaire, 3 Allée La Boëtie, F33600 Pessac, France

(Received 30 November 1993; revised version received 7 March 1994; accepted 11 April 1994)

Abstract

Fibered Si–C–N–O-based ceramics from a polycarbosilazane precursor (copolymer) are studied, then compared to other ceramic materials previously prepared and described in other papers. The emphasis is upon the structural and textural features as observed by high-resolution transmission electron microscopy and their evolution with an increasing heat-treatment temperature up to 1600°C. Both argon or nitrogen atmospheres were used. Specifically, the peculiar behavior of the material during the amorphous to crystalline transition until degradation is revealed. The consequences on the nucleation and the growth of the SiC grains, and the electrical and mechanical properties are discussed.

Faserverstärkte Si–C–N–O–Keramiken, hergestellt aus einem neuen Polykarbosilizanvorläufer (Copolymer) wurden untersucht und mit anderen Keramiken verglichen. Der Schwerpunkt liegt auf der Untersuchung der Struktur und Textur mittels hochauflösender Transmissionselektronenmikroskopie und ihrer Entwicklung mit zunehmender Wärmebehandlungstemperatur bis zu 1600°C in einer Argon- oder Stickstoffatmosphäre. Speziell das eigentümliche Verhalten des Materials während des Übergangs vom amorphen in den kristallinen Zustand bis zur Degradation konnte aufgeklärt werden. Die Auswirkungen auf die Keimbildung und das Wachstum der SiC-Körner und die elektrischen und mechanischen Eigenschaften werden diskutiert.

On étudie des céramiques de géométrie filamentaire appartenant au système Si–C–N–O et élaborées à partir d'un précurseur copolymère de type polycarbosilazane. L'accent est mis sur les caractéristiques structurales et texturales révélées par microscopie électronique par transmission à haute résolution, et sur leur évolution au cours d'un traitement thermique croissant jusqu'à; 1600°C. En particulier, le comportement du matériau durant la transition amorphe–cristal jusqu'à dégradation s'avère très spécifique, et ses conséquences sur la nucléation puis la croissance des cristaux de SiC, ainsi que sur les propriétés électriques et mécaniques sont discutées

1 Introduction

The limitation of the thermal stability of the polymer-derived Si–C–O-based ceramic fibers, either commercial (Nicalon NL-200 type) or laboratory made, has resulted in the need to look for new developments. Searching for new oxygen-free reticulation routes has been among the possible routes for research. Another main direction has been to look for new polymeric precursors including chemical elements hopefully able to allow the oxygen curing step to be avoided, or able to improve the thermal stability at least. In this regard, nitrogen-containing polymers have been tried.[1–9]

Unfortunately, incorporating nitrogen does not succeed in preventing the fibers from melting, after spinning during the ceramization step.

Therefore, a curing step is still necessary. Moreover, nitrogen in ceramics from the Si–C–N system has been found to play a similar role to oxygen. Specifically, nitrogen is present in a SiC_xN_y intergranular phase (together with a polyaromatic carbon network) between SiC crystal.[10] When the SiC_xN_y phase thermally degrades, it is also able to induce a chemical degradation of the carbon phase. However, in spite of their similar behavior, Si–C–N-based ceramics appear thermally more stable than Si–C–O-based ceramics.[10] Therefore, it was important to check how stable the Si–C–N–O-based fibers derived from a polycarbosilazane precursor were, compared to Si–C–O-based fibers, and, more generally, to understand their thermal behavior and to determine their way of thermal degradation.

This paper reports part of a wider study in which many physical and chemical aspects have been investigated by several laboratories. The authors own work is focused on the structural, micro- and nanotextural features of the ceramics, as obtained from high-resolution transmission electron microscopy (HRTEM),[10–13] and their relationships with some subsequent physical properties.

2 Experimental

2.1 Samples

Samples were prepared from a polycarbosilazane (PCSZ) copolymer route described elsewhere.[4] Briefly, the PCSZ precursor was prepared by the Laboratoire de Chimie Organique et Organométallique (Bordeaux, France) from the condensation of various proportions of dichlorosilane and dimethyldichlorosilazane (in toluene, with sodium) to give a polysilasilazane (PSSZ) with various x values (Fig. 1). Thermolysis (350–500°C) of the PSSZ allows CH_2 groups to insert between two Si atoms, changing it into a polycarbosilazane (PCSZ). The fibers studied here were prepared from the PSSZ precursor with $x = 0{\cdot}5$ following a melt spinning route. The as-spun fibers were cured by using a mixture of gaseous nitrogen and oxygen at a temperature below 200°C.[14] The materials were then heat treated up to 850°C under argon (300°C/h). At this temperature the weight loss has become negligible and the ceramization of

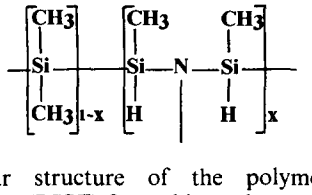

Fig. 1. Molecular structure of the polymeric precursor (PSSZ) from this study.

the material is achieved. The chemical changes occurring during the ceramization stage have been studied elsewhere.[15] At 1000°C, the chemical composition of the ceramized fiber is $SiC_{0{\cdot}8}N_{0{\cdot}4}O_{0{\cdot}6}$. The thermal stability of the fibers was then investigated through further heat treatments under pure nitrogen or argon flow at various temperatures T_p up to 1600°C at 3600°C/h. (15 min, isothermal).

2.2 Analytical procedures

TGA analysis (SETARAM TAG 24) were performed at 600°C/h on the starting material (i.e. the 850°C ceramized fiber) in a graphite crucible under purified argon flow.

Elemental analysis was performed with an electron probe microanalysis (EPMA, with a CAMEBAX 75) on a polished metallographic cross-section. The hydrogen contents were not able to be estimated by this technique.

The electrical conductivity σ was measured from room temperature up to θ = 600°C under helium atmosphere. The measurements were performed on 10 monofilament tow sets on alumina plates. The electrical contacts were secured with a silver lake. Because of the semiconductor behavior of the materials, electrical properties were mainly followed through the variation of the apparent activation energy E_a with T_p (calculated from the slope of the $\log_{10} \sigma = F(1/\theta)$ graphs). The σ values given in Table 1 are taken at θ = 230°C rather than at room temperature to avoid any possible machine effect. Because only the shape factor of fibers was able to be known, only the conductivity values of fibers can be compared in Table 1.

Before HRTEM examination (Philips EM 400, 120 kV) samples were embedded in epoxy resin then sliced with a diamond knife (cross-sections) using a LKB microtom. Convenient thicknesses of samples thus prepared were around 50 nm. The sample foils were gathered on a copper grid coated with either a holey or continuous thin film (<10 nm) of amorphous carbon. The principles of the HRTEM investigations have been previously described.[11–13] Briefly, in addition to the bright field (BF), electron diffraction (SAD) and lattice fringe (LF) modes, which were used following common procedures, a specific dark field (DF) procedure was performed. By displacing radially or azimuthally the diffraction pattern relative to the objective aperture, successive dark field images may be obtained, providing information on the relative location and orientations of the various phases of which the material is made. To summarize, position 1 (DF1) will specifically image a carbon phase (if any) made of polyaromatic layer stacks seen edge-on, and position 2 (DF2)

Table 1. Electrical conductivity σ (measured at θ = 500K) and apparent activation energy E_a versus increasing T_p (argon atmosphere) for Si–C–O[13,27] and Si–C–N–O fibers

		T_p (°C)					
		850	*1000*	*1200*	*1250*	*1400*	*1450*
Si–C–N–O							
	σ $(\Omega.cm)^{-1}$	—	10^{-8}	10^{-6}	—	$10^{-2.5}$	$10^{-1.5}$
	E_a (eV)	—	1·100	0·770	—	0·055	0·040
Si–C–O							
	σ $(\Omega.cm)^{-1}$	3×10^{5}	—	$6{\cdot}3 \times 10^{-4}$	1	1·5	—
	E_a (eV)	0·660	—	0·330	0·050	0·010	—

will image SiC crystals (if any) oriented so as to provide a 111 or 200 reflection (for the cubic structure).

3 Physicochemical

The weight loss (Ar atmosphere) for the ceramized fibers is reported in Fig. 2, as compared with ceramized Si–C–O- (fibers) or Si–C–N- (bulk) based ceramic materials. The weight loss is very low up to about 1450°C, then it reaches 50% beyond 1500°C. This behavior is sustained by the chemical composition (Table 2) which remains unchanged up to 1450°C for heat treatment under argon. However, the elemental analysis data are obtained from EPMA measurements, carried out on the center part of the fibers. In fact, SEM and TEM images (see later) show that a skin/core effect occurs between 1200 and 1450°C and proceeds with the increasing temperature. At 1600°C under argon, the fibers have lost almost all their oxygen and nitrogen content, and the overall composition tends towards the SiC stoichiometry.

In contrast, at 1600°C under nitrogen, the nitrogen content is maintained in the material, and the oxygen loss is less (Table 2). This goes with a lower weight loss.[15] The fact that only the N content increases consecutively to the oxygen loss suggests a concomitant release of SiO and CO.

Considering on the one hand the thermal stability of crystallized Si_3N_4, and on the other hand the initial N/Si atomic ratio of the bulk which is by far very low relative to the N/Si atomic ratio for Si_3N_4 (0·38 compared to 1·33), the data in Table 2 already indicate that the occurrence of Si_3N_4 crystals has probably not been possible in the fibers

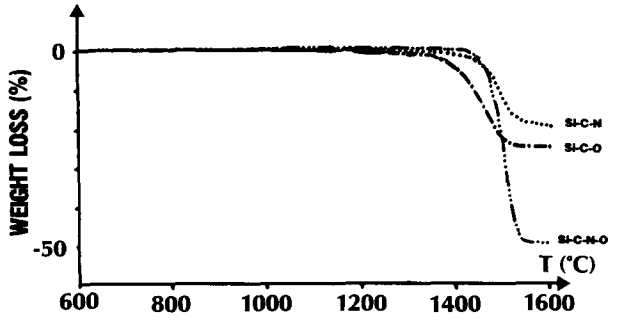

Fig. 2. Weight losses recorded from TGA for the Si–C–N–O system (fibers) compared to the Si–C–O (fiber) or Si–C–N (bulk) systems.

Table 2. Elemental analysis (from EPMA) for the Si–C–N–O fibers with the increasing heat-treatment temperature T_p. At 1400 and 1450°C, and 1450°C, due to the occurrence of a sheath at the outer part of the fibers, the analysis was performed on the core only

Atmosphere	T_p (°C)	*Si (at.%)*	*C (at.%)*	*O (at.%)*	*N (at.%)*
Ar or N_2	1000	36	29	21	14
	1200	36	28	22	14
	1400	36	28	22	14
	1450				
Ar	1600	49	50	0·5	0·5
N_2	1600	36	31	7	26

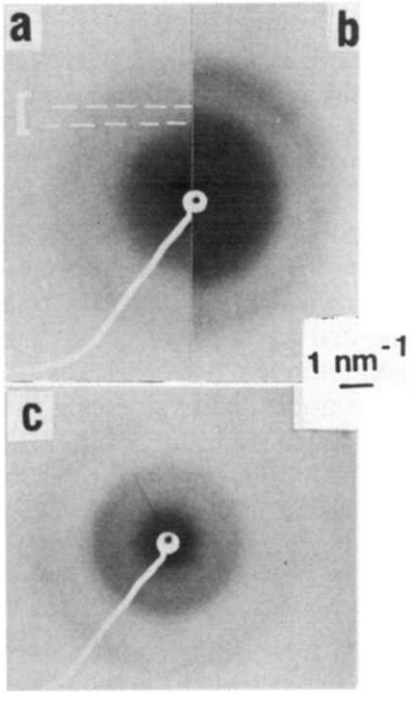

Fig. 3. Selected area diffraction (SAD) patterns (a) from the Si–C–N–O fiber for T_p = 1200 (bulk), 1400 and 1450°C (core); (b) from an amorphous Si–C–N phase derived from a polyvinylsilazane;[12] (c) from an amorphous Si–C phase derived from a polycarbosilane.[13]

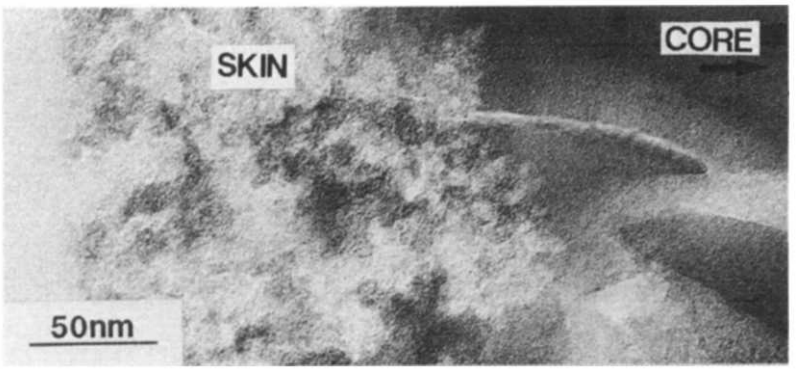

Fig. 4. Bright field image of a cross-section of the outer part of the fiber. T_p = 1400°C. The fiber skin is on left. The elongated morphology in the fiber core is a microtomy artifact.

(at least under argon heat treatment). Likewise, the low initial C/Si atomic ratio (0·8) leads to the supposition that the free carbon phase is not, or will not be, well developed compared to other systems.

Comparing the weight loss of the Si–C–N–O system with Si–C–N and Si–C–O systems (Fig. 2) indicates on the one hand that nitrogen-containing systems are more stable than nitrogen-free systems, and on the other hand that oxygen-free systems lose less weight than oxygen-containing systems.

3.1 Structural and textural (HRTEM)

3.1.1 Heat treatment under argon

Up to T_p = 1200°C at least, the fiber exhibits a nanometric porosity as in other polymer-based ceramic materials.[10–13,16,17] The material is amorphous (Fig. 3(a)) and closer to a Si–C-type phase (Fig. 3(c)), i.e. characterized by a diffuse plateau or a halo ending at about 3·9–4 nm^{-1} (in addition to a faint halo at 6·87 nm^{-1}), than to a Si–C–N-type phase (Fig. 3(b)) characterized by a diffuse plateau ending at 5 nm^{-1}.

At T_p = 1400°C, a core/skin effect occurs, as revealed by an obvious microtextural discrepancy (Fig. 4). The sheath, the thickness of which is about 0·2 μm, now exhibits a pore size much larger than that of the inner part. This textural modification undoubtedly reveals the beginning of the chemical modification involving the degradation of the $SiC_xN_yO_z$ continuum of which the material is mainly made, referring to previous work on other polymer-based ceramic materials.[18–21] The degradation subsequently induces the high weight loss observed through TGA measurements (Fig. 2).

Surprisingly, the textural difference does not go with structural changes, and the overall SAD patterns of the core or the skin as well remain similar to that of Fig. 3(a). However, a carbon phase has occurred, the quantity of which is too low and the structural organization of which is too poor to be detectable on the SAD patterns. The occurrence of small polyaromatic stacks of carbon clusters either in the core or in the skin is attested to by a focus series in the DF1 image mode, as already performed for other polymer-

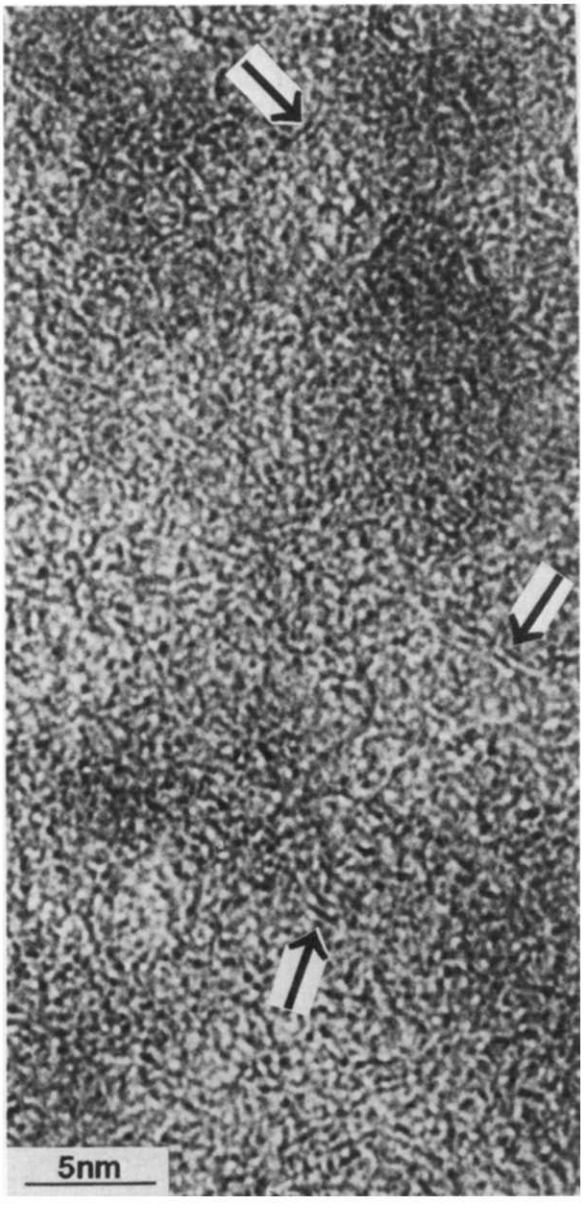

Fig. 5. Lattice fringe image of the sheath of the fiber. Arrows indicate some altered BSUs. Note the overall nanoporous texture.

Fig. 6. SEM image of a fiber for T_p = 1450°C. The thickness of the skin has increased, and the skin easily desolidarizes from the core.

based ceramic materials.[13] Nevertheless, the nanotexture of carbon in the outer part is somewhat different from the inner part. In the latter, carbon is present as BSUs (basic structural units, i.e. small stacks (almost isometric ~1 nm) of 2–3 polyaromatic layers piled up face-to-face), which are the common primary form of carbon in polymer-based ceramic materials.[11,13,16] In the former, carbon seems to be altered into a porous and channeled nanotexture (Fig. 5), as encountered in some carbon fibers activated through a 'soft' oxidation procedure.[22]

At T_p = 1450°C, the skin/core effect has proceeded quickly, so as to be revealed by mere SEM examinations (Fig. 6). The core of the fiber is structurally and texturally identical to the core of the 1400°C heat-treated fiber, i.e. mainly amorphous but containing BSUs. The thickness of the sheath may vary from at least 0·3 to 3 μm from one fiber to another or along the same fiber as well. Such a wide range of thickness values reveals a fast kinetic rate and may possibly be explained by the location of the fibers relative to each other within the oven and/or an interaction effect between neighboring fibers, inducing local differences in gas partial pressures, heat transfers, etc. Contrarily to the 1400°C heat-treated fiber, SiC crystals are now numerous (Fig. 7(a) and (b)), but

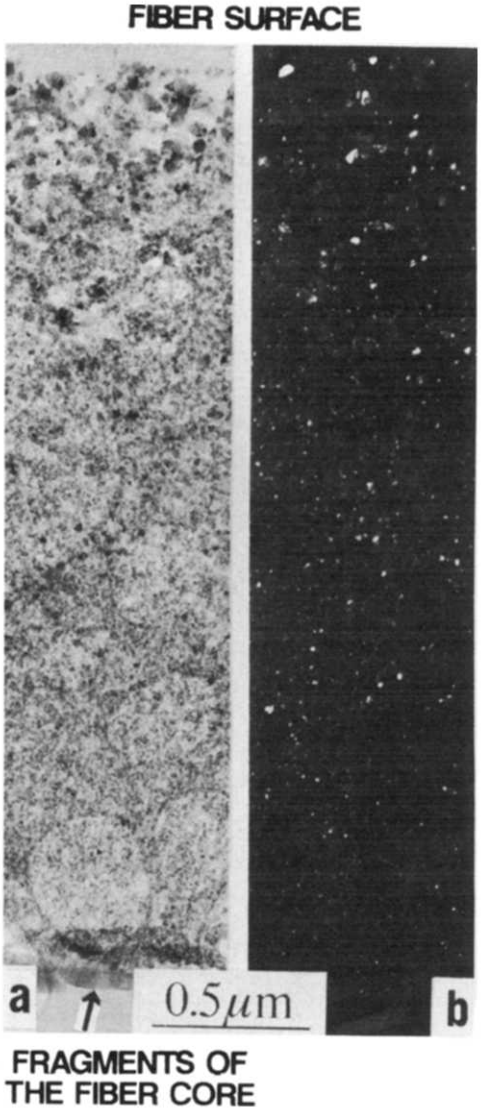

Fig. 7. Images of the fiber skin (cross section) for T_p = 1450°C. (a) Bright field image. (b) Position 2 dark field image (DF2).

in the outer part (skin) only. When the skin is thick (3 μm for instance), it clearly appears that the crystal sizes are distributed following a decreasing gradient from the fiber surface to the skin/core interface (Fig. 7(b)). The gradient of crystal sizes induces changes in the SAD patterns. Diffraction rings from a zone close to the fiber surface are sharper and dotted (Fig. 8(a)) while diffraction rings from a zone close to the skin/core interface are broader and continuous (Fig. 8(b)). Both (Fig. 8(a) and (b)) indicate a SiC phase from the β structure. However, some marks of polytypism occur for the biggest crystals, i.e. close to the surface (Fig. 8(a), arrow). In the outer part of the skin, maximal sizes for SiC crystals are 45 nm, while only 10 nm in the inner part of the skin. In both cases, the size range is wide.

Since the occurrence of the skin reveals the beginning of chemical changes in the fiber, the thickness of the skin and the mean crystal size increase as the chemical changes proceed. This is a re-

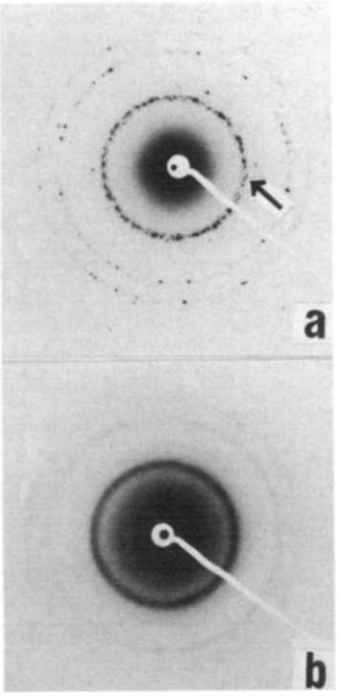

Fig. 8. SAD patterns from the fiber skin for T_p = 1450°C (a) close to the surface; the arrow indicates a polytype SiC crystal; (b) close to the skin/core interface.

minder of similar behavior observed for Si–C–O-based ceramic fibers.[13,16] However, a discrepancy between Si–C–O fibers and the present Si–C–N–O fibers lies in the crystal shapes. Although mainly from the β structure in both samples, the SiC crystals are always isometric in Si–C–O fibers, while their in-plane projection often exhibits a triangular shape in Si–C–N–O fibers (Fig. 9(a) or (c)). It should be noted that free carbon, as altered BSUs similar to that described in the skin of the 1400°C heat-treated fiber, is no longer dispersed but—of course—concentrated around the SiC crystals (Fig. 9(b)). Close to the skin/core interface, because SiC crystals are very small the microtexture is porous and channelled, as for T_p = 1400°C (Fig. 10). On the contrary, intact BSUs are visible in the non-altered core of the fiber (Fig. 10, arrows).

EELs measurements bring some information on the chemical changes occurring from the fiber periphery (Table 3). The good agreement between

Table 3. Some atomic ratios from EELS measurements for Si–C–N–O-based fibers heat-treated under nitrogen or argon

Atmosphere	T_p (°C)		*Atomic ratio*		
			O/Si	*N/Si*	*C/Si*
Argon	1 450	Core	0·6	0·3	0·7
		Skin	$0{\cdot}3_6$	0	2
	1 600	Bulk	0	0	1·1
Nitrogen	1 400	Core	0·8	$0{\cdot}5_4$	1·8
		Skin	0·5	0·7	$1{\cdot}7_5$
	1 600	Bulk	0	$0{\cdot}4_8$	$1{\cdot}5_6$

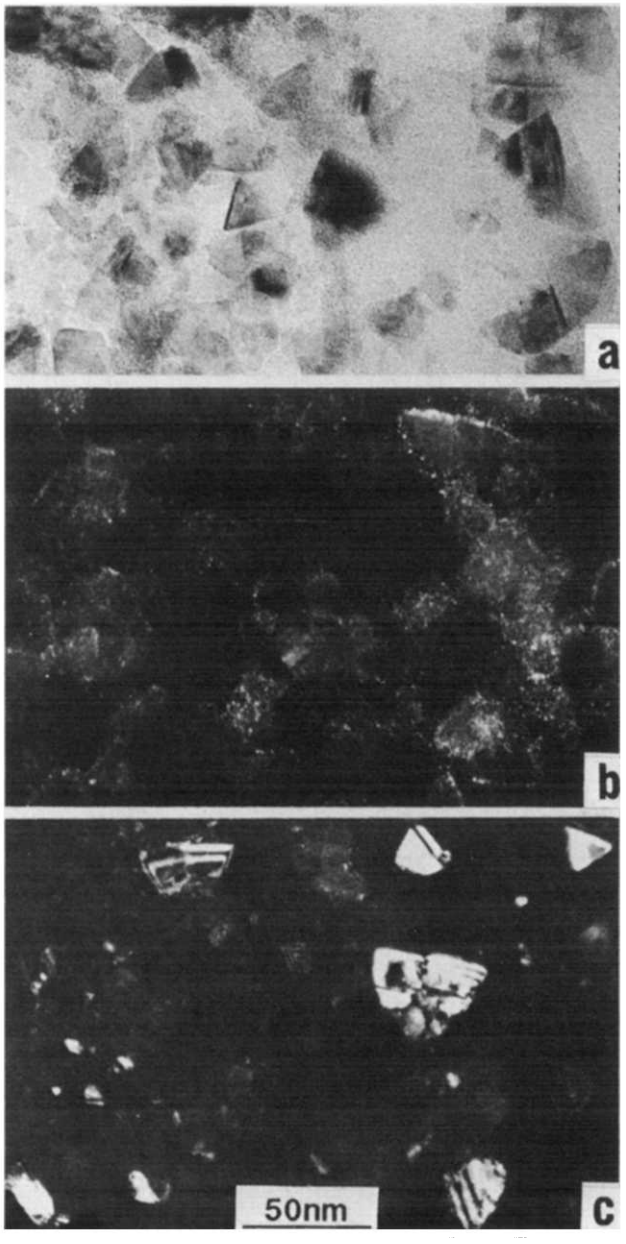

Fig. 9. Outer part of the fiber skin (cross section) for T_p = 1450°C. (a) Bright field. (b) Position 1 dark field image revealing altered carbon (bright dots) around the SiC crystals. (c) Position 2 dark field image revealing some SiC crystals.

the atomic ratio values O/Si, N/Si and C/Si obtained from the fiber core by EELS (0·6, 0·3 and 0·7 respectively) and by EPMA (0·61, 0·38 and 0·77 respectively, see Table 2) for T_p = 1450°C validate the reliability of the measurements. As mentioned in Section 3.1, the chemical composition has not changed compared to T_p = 1200°C, indicating that the fiber core is stable. On the contrary, nitrogen has completely disappeared in the skin, together with only a part of the oxygen. Correspondingly, the skin is relatively enriched in carbon. However the C/Si ratio (and maybe O/Si) given in Table 3 (C/Si = 2) is possibly overestimated due to a contribution of the embedding epoxy resin somewhat filling the porosity. Anyway, the O/Si value indicated for the skin at T_p = 1450°C (Table 3) is in fact a mean value, since the

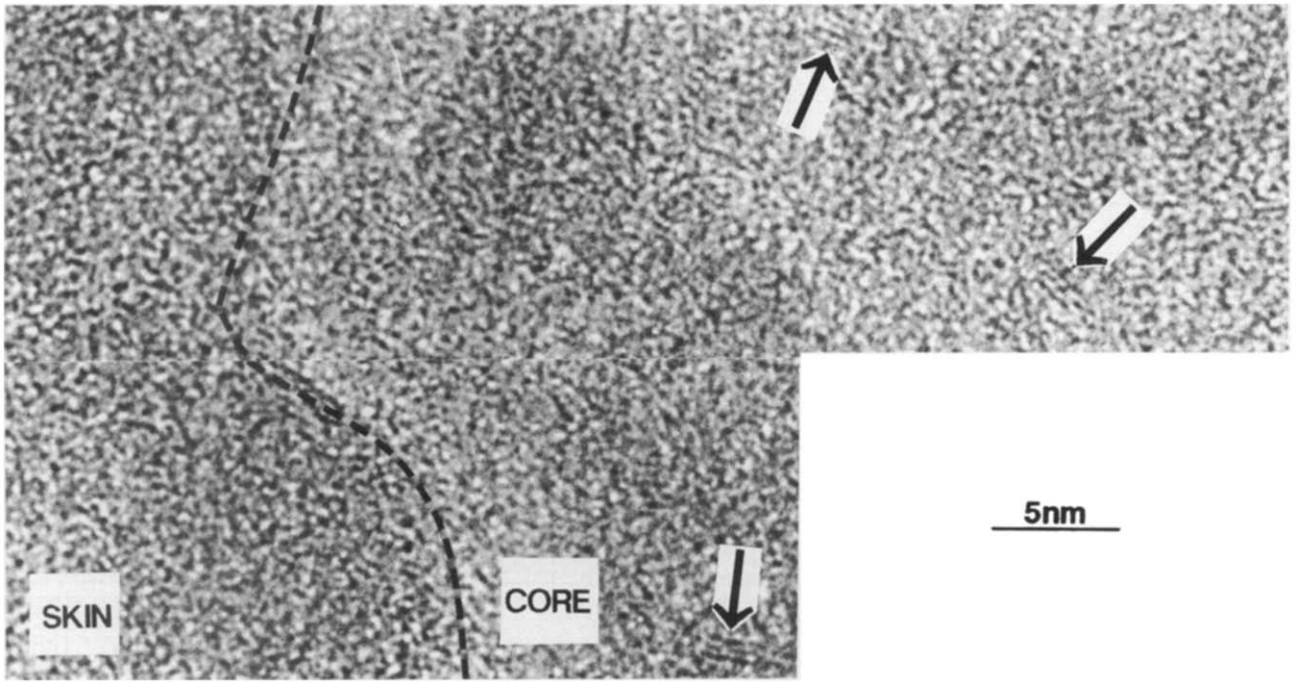

Fig. 10. Lattice fringe image. Skin/core interface of the fiber for T_p = 1450°C. Arrows indicate unaltered BSUs.

real value has been found to decrease continuously from the skin/core interface to the fiber surface. This effect has to be related with the increasing size of SiC crystals. Such a direct relationship between the decrease in oxygen content and the increase in SiC grain size has already been found in Si–C–O fibers.[17]

For T_p = 1600°C, the fiber has become homogeneous and the chemical degradation has invaded the whole fiber (Fig. 11). The overall grain growth has proceeded (Fig. 12). The modal size (i.e. the most frequent) is 15–20 nm, with maximal values around 90 nm. Triangular shapes for crystals are still present but seldom (Fig. 13), and most of the crystals have become isometric. Free carbon is absent or rare. N/Si, O/Si and C/Si atomic ratios from EELS are given in Table 3. Again, the agreement with EPMA measurements is good, and both analyses (Tables 2 and 3) indicate that O and N have been removed and that the overall compositions tend toward the stoichiometry of SiC, through the probable loss of gaseous moieties such as CO and SiO, among others.

3.1.2 Heat treatment under nitrogen

At T_p = 1400°C, features are identical to the fibers heat-treated under argon, although the skin thickness is thinner (0·1–0·15 μm). The main discrepancy is chemical, since EELS measurements confirm the bulk data obtained from EPMA and indicate that nitrogen is still present in the skin. The N/Si ratio is even

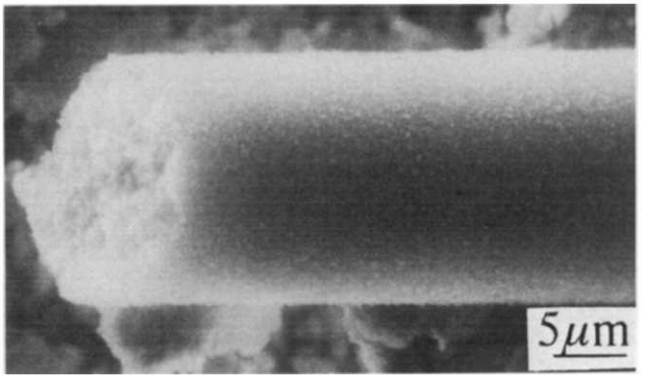

Fig. 11. SEM view of a fiber for T_p = 1600°C. The skin/core effect is no longer visible.

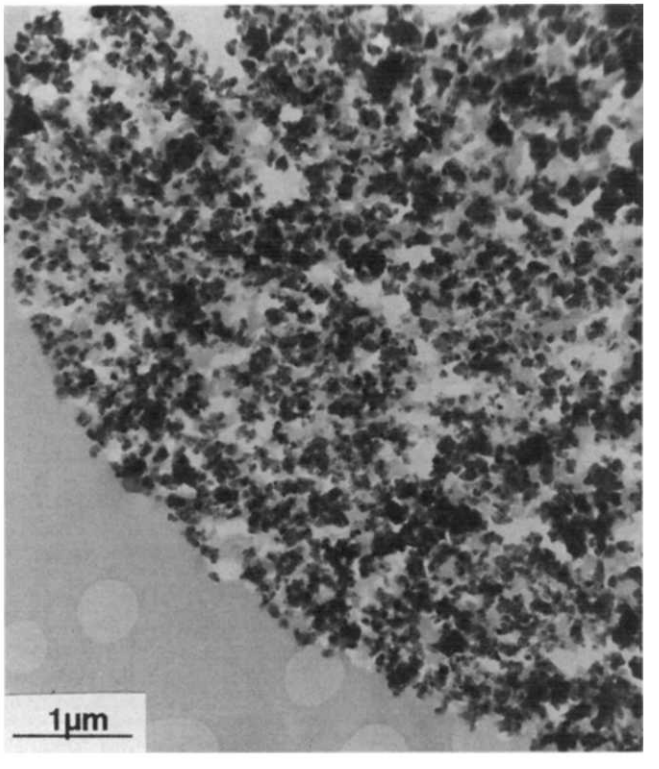

Fig. 12. Bright field image of part of the fiber (cross-section) for T_p = 1600°C.

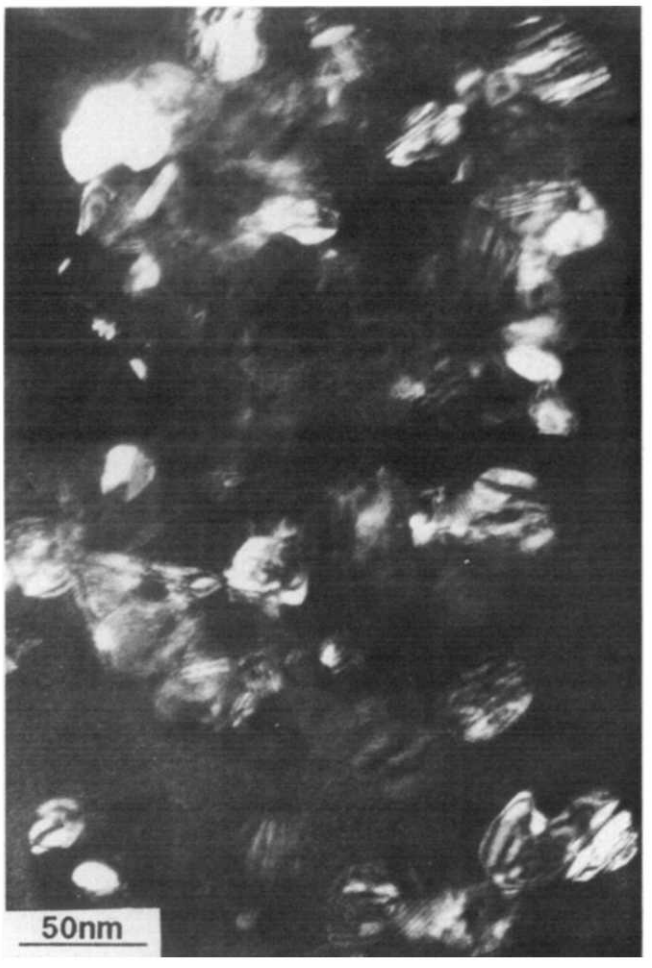

Fig. 13. Position 2 dark field image of part of the fiber (cross-section) for T_p = 1600°C. Crystals are SiC.

higher in the skin than in the core, probably because of the relative increase due to the oxygen release as SiO and probably CO as well. However, only the tendencies have to be considered, since the accordance with EPMA data (Table 2) is rather poor.

For T_p = 1450°C, the chemical degradation has proceeded and the skin thickness has increased to 0·4–0·5 μm (Fig. 14(a)). However, this thickness remains lower than the thickness of the argon heat-treated fibers. The main difference is now structural. Contrarily to the argon experiments, the SiC crystallization has not yet occurred in the skin (Fig. 14(b)).

For T_p = 1600°C, the fiber has become homogeneous since the skin has invaded the whole volume (Fig. 15). The SiC phase has finally crystallized (Fig. 16(a)). The modal size of crystals is 1–2 nm, for a maximal size at 4 nm (Fig. 16(b)). A reverse grain size gradient is observed, compared to argon experiments, i.e. SiC crystal sizes slightly decrease from the core to the fiber surface. The carbon phase is now degraded everywhere. EELS measurements are reported on Table 3. They show that nitrogen is just starting to leave the system, while oxygen is now no longer present. Another specificity of the 1600°C heat-treated fibers under nitrogen is the occurrence of numerous needle-like crystals, the locations and proportions of which are related to the position of the fibers relative to furnace geometry (Fig. 17(a) and (b)). TEM images indicate a conical morphology and a fault-free structure (Fig. 18), actually different from that of a SiC whisker. EELS measurements identify them as Si_3N_4 crystals (atomic N/Si ratio = 1·4), the structure of which has been determined through DEAS patterns as α-Si_3N_4 (α can be distinguished from β by the presence of reflections at 0·432 and 0·259 nm, and the absence of reflection at 0·267 nm). These crystals are electron (or heat)

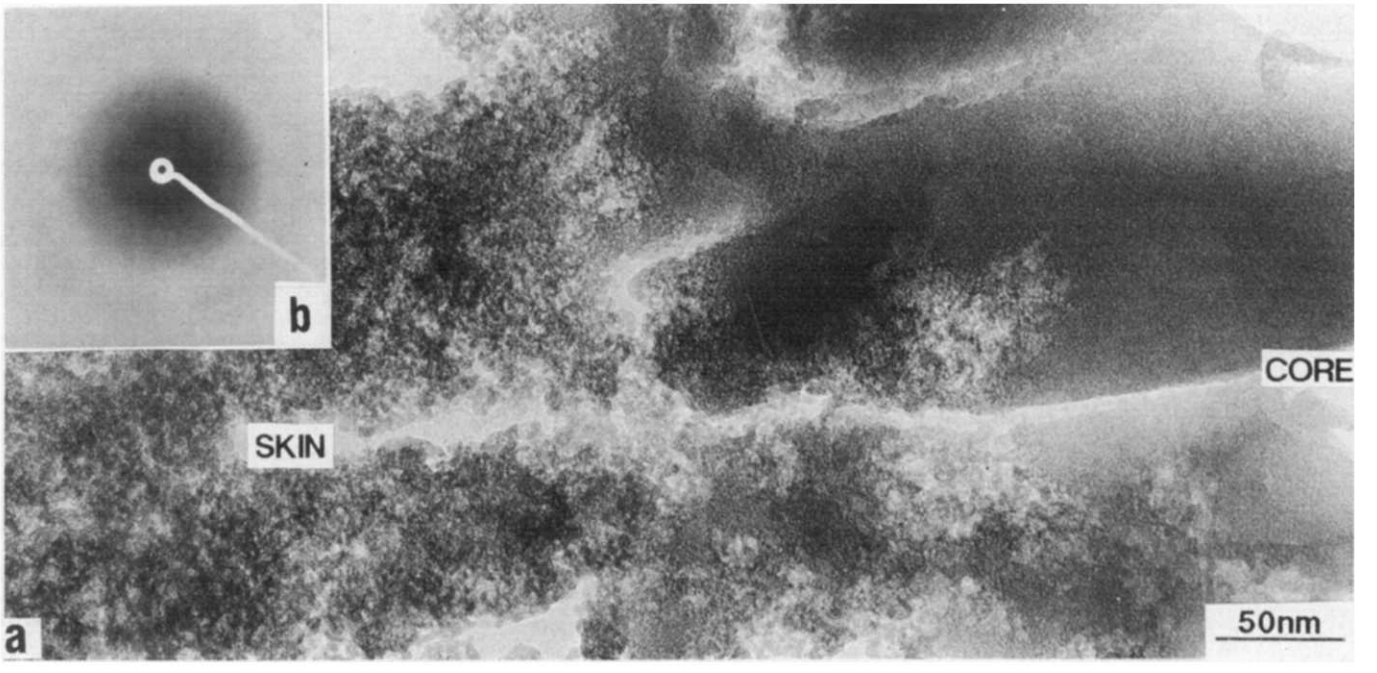

Fig. 14. Experiments under nitrogen. Outer part of the fiber (cross-section) around the skin/core interface for T_p = 1450°C. (a) Bright field. (b) SAD pattern revealing the amorphous structure.

Fig. 15. Experiments under nitrogen. Overall view of the cross-section of the fiber. T_p = 1600°C. The skin/core effect is no longer visible.

sensitive and sublimate as soon as the electron beam is highly focused on them.

4 Discussion

Briefly, the thermal behavior (inert atmosphere) of the PCSZ-derived fiber may be summarized as follows:

Stage 1 (<1400°C): The material is amorphous, and the overall structure is close to that of amorphous SiC. A carbon phase occurs as BSUs. O and N are involved in an amorphous $SiC_xN_yO_z$ continuum.

Stage 2 (1400–1600°C): Oxygen and (mainly) nitrogen escape progressively as gaseous species, following a chemical reaction which proceeds from the fiber surface to the fiber core. In the meantime, the carbon phase is altered and the SiC crystals nucleate, then grow up. The material tends to be made of SiC crystals, altered carbon, and a residual $SiC_xN_yO_z$ intergranular phase.

Stage 3 (≥ 1600°C): The material is polycrystalline and no longer has any oxygen or nitrogen content. Its overall chemical composition tends towards stoichiometric SiC.

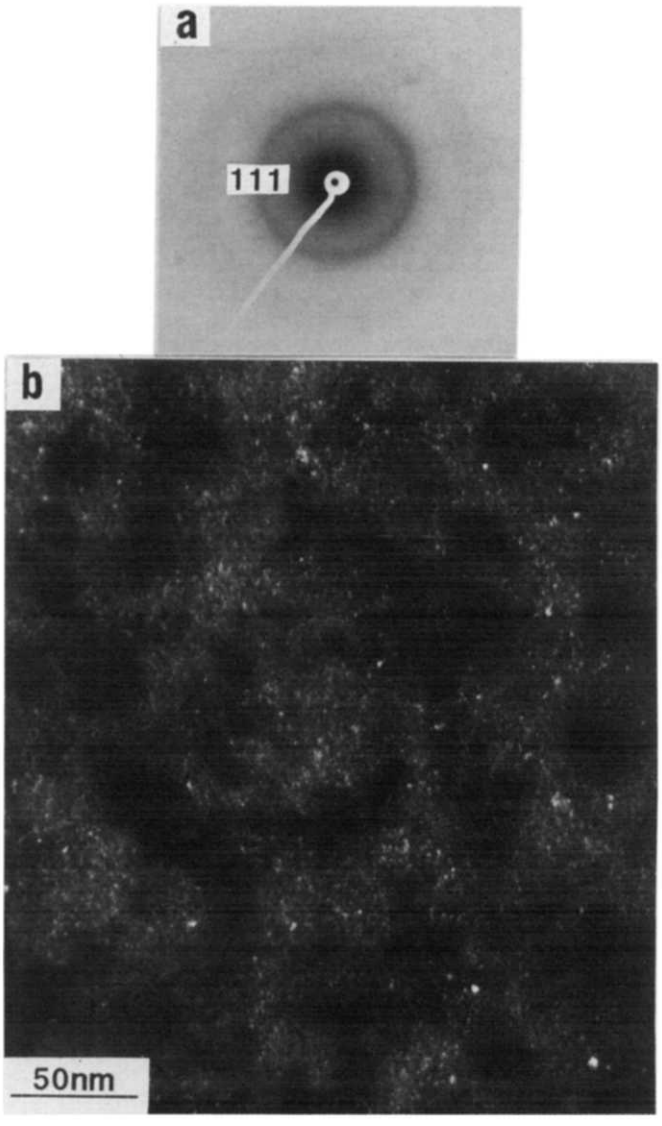

Fig. 16. Experiments under nitrogen. T_p = 1600°C. (a) SAD pattern exhibiting the β-SiC features. (b) Position 2 DF image revealing the small size of SiC crystals.

Thus, the degradation reaction of the chemical bonds involving O and N controls the thermal evolution of the material. Since the degradation reaction produces gaseous species (CO, N_2[15] and probably SiO), it is controlled by the partial pressure of gases. Of course, the degradation reactions will occur more quickly at the fiber surface where the partial pressures of gases remain low, than in the fiber core where gas diffusion is controlled by the porosity. Therefore, as for Si–C–O-based fibers,[13,16,23] the thermochemical degradation of the material and the subsequent grain growth will proceed from the outer part to the inner part of the fiber, inducing a core/skin texture for a while.

4.1 Comparison with polymer-based ceramics from ternary systems (Si–C–N and Si–C–O)

Adding oxygen (Si–C–N–O system) clearly delays the SiC nucleation from 200–300°C relative to a Si–C–N-based ceramic from the same polymer.[10] Relative to a Si–C–O-based ceramic,[13] adding

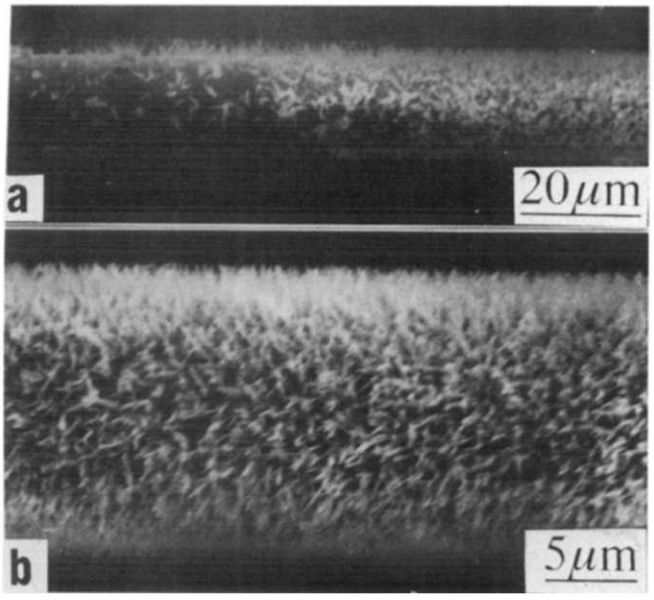

Fig. 17. Experiments under nitrogen. (a) and (b) SEM views of fibers for T_p = 1600°C.

nitrogen also seems to delay the SiC nucleation, but less efficiently (from about 100°C only). In all the systems, the degradation of the amorphous continuum (SiO_xC_y, SiC_xN_y or $SiC_xN_yO_z$, depending on the system) is controlled by the partial pressures of the gases released. However, the Si–C–N–O system is the only system for which the degradation of the continuum starts before the SiC nucleation. This could explain why the SiC grain growth also seems to follow a different mechanism. Indeed, in any Si–C–O or Si–C–N ceramic material derived from PCS or PCSZ until now,[10–15] (including Nicalon fiber[16–17]), the grain growth is following two paths. The first path is slow, the grain growth being controlled by the possibilities of structural rearrangements at the grain boundaries or within the continuum surrounding the crystals. The second path is fast and consecutive to the degradation of the continuum. The quick disappearance of both the intergranular phases (the continuum and the carbon phase) then allows the SiC grains to coalesce by impingements. The resulting crystals have always in-plane projections which exhibit isometric shapes, suggesting crystalline forms belonging to a combination of tetrahedral {111}, inverse tetrahedral $\{\bar{1}\bar{1}\bar{1}\}$, cubic {100} and rhomboïdal dodecahedral {110} types. In contrast, the mechanism of crystal growth is different in Si–C–N–O fibers, as suggested by the occurrence of a gradient of grain size within the skin (not found in Si–C–O laboratory-made fibers[15] or Nicalon fibers[16]). Moreover, in-plane projections of crystals often exhibit triangular shapes (Fig. 9(a) and (c) and Fig. 13), revealing crystalline forms from the {111} (tetrahedral) type. The growth mechanism is thus able to respect the relative expansion rate of the various crystal faces of the face centered cubic, promoting the 'slow' faces (111) to the detriment of the 'fast' faces (100) and (110). Such a feature is specific from a slow rate growth such as a nucleation-then-growth mechanism, which is possibly close, due to the high temperatures (>1400°C), to an Ostwald mechanism (atom-by-atom growth).

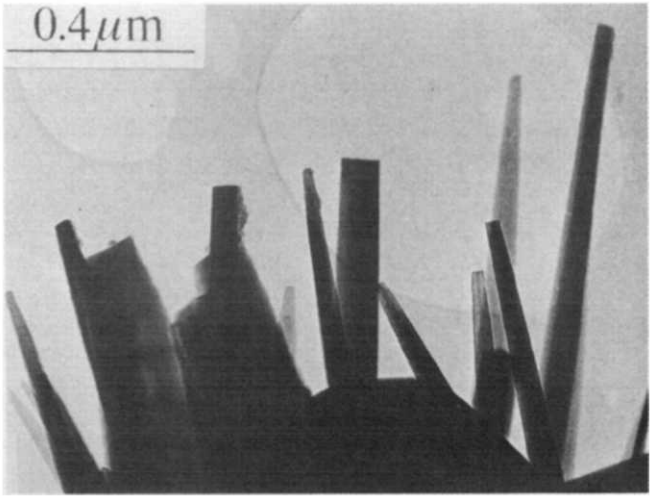

Fig. 18. Experiments under nitrogen. T_p = 1600°C. Bright field image of the outer needle-like Si_3N_4 crystals coating some parts of the fiber.

4.2 Influence of a nitrogen atmosphere

The thermal behavior of the fiber is different from that of argon experiments and may be summarized as follows:

Stage 1 (< 1400°C): Assumed to be identical to the argon experiment (samples have not been investigated).

Stage 2 (1400–1600°C): Skin/core effect similar to the argon experiment. However, only oxygen escapes (together with Si and C, as gaseous SiO and CO). The structure is amorphous both for the skin and the core. Carbon is present as BSUs in the core, and is altered in the skin.

Stage 3 (≥ 1600°C): The oxygen loss is achieved and the nitrogen loss is only starting. In the meantime, β-SiC crystals nucleate, then grow up in the bulk, while α-Si_3N_4 needle-like crystals occur at the fiber surface.

Thus, using a nitrogen atmosphere prevents the release of the intrinsic nitrogen from the fiber, which confirms that gaseous N_2 is involved as by-product from the degradation reactions of the fiber.[15] Elemental analysis data also suggest the release of gaseous SiO (and CO[15]). As oxygen is leaving the system, the inhibition of the Si nucleation is insured by the presence of nitrogen atoms as a reticulating agent in the residual continuum. This explains why the SiC nucleation is controlled

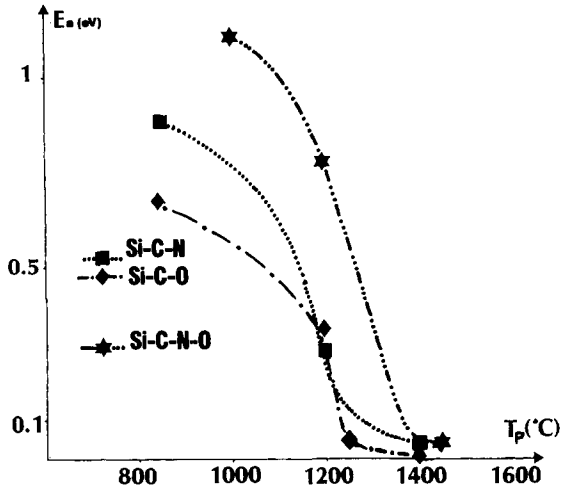

Fig. 19. Apparent activation energy E_p for conductivity versus increasing T_p for the ceramics from (♦) Si–C–O, (■) Si–C–N and (★) Si–C–N–O systems.

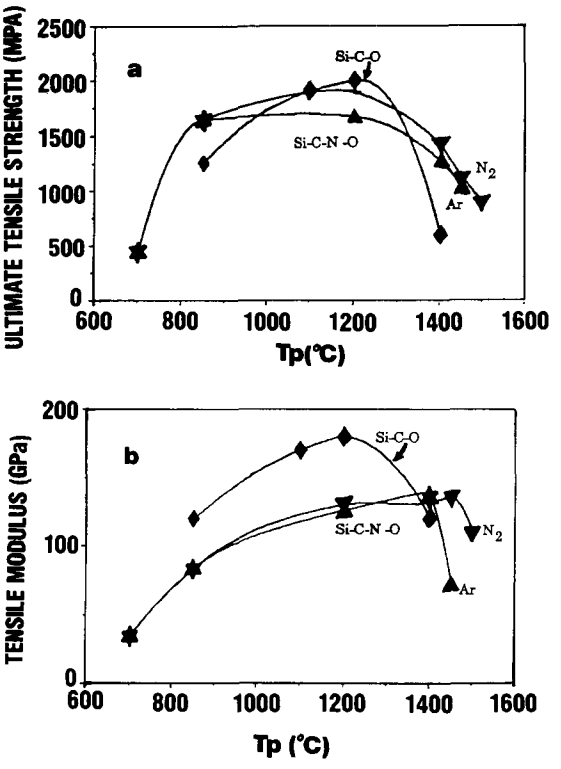

Fig. 20. (a) Ultimate strength values and (b) elastic modulus values for both argon or nitrogen heat-treated Si–C–N–O fibers or argon heat-treated Si–C–O fibers versus increasing T_p.

by the release of gaseous N_2 from the material, itself influenced by the presence of a N_2 atmosphere. Such a control effect is sustained by the occurrence of a gradient of crystal sizes, which decreases from the core to the surface for T_p = 1600°C (i.e. the gradient is inverse from the argon experiments). Indeed, the control effect by the N_2 atmosphere necessarily also follows a decreasing gradient from the outer part to the inner part of the fiber since it depends on its diffusion through the porosity. The N/Si atomic ratio is never high enough (0·48 for the highest) to allow Si_3N_4 crystals to nucleate within the fiber. On the contrary, the occurrence of Si_3N_4 whiskers at the fiber surface suggests a vapor growth mechanism following reactions such as:[24–26]

$$3\ SiO_{(g)} + 3\ CO_{(g)} + 2\ N_{2(g)} \rightarrow Si_3N_{4(s)} + 3\ CO_{2(g)}$$

or

$$3\ Si_{(g)} + 2\ N_{2(g)} \rightarrow Si_3N_{4(s)}$$

or

$$3\ SiO_{(g)} + 2\ N_{2(g)} \rightarrow Si_3N_{4(s)} + 3/2\ O_{2(g)}$$

4.3 Relationships with electrical and mechanical properties

Compared to the Si–C–N and Si–C–O systems, the behavior of which is commented on in related papers,[10,13,14] the main change in conductivity of the Si–C–N–O fibers (as followed by the apparent activation energy E_a, see Section 2.2.) also occurs between 1200–1250°C and 1400°C (Fig. 19). As previously discussed,[27] this corresponds to a semiconductor/semi-metallic transition. Again, the only structural change which could explain this behavior is the nucleation of the carbon phase, though only at the BSU state. The fact that BSUs have not the time to associate into a network before the overall degradation of the fiber could explain that the conductivity values are lower than the values for the Si–C–O fiber (Table 1).

Figure 20(a) indicates that the ultimate tensile strength values decrease in the 1200–1400°C temperature range for both fibers heat treated under argon or nitrogen. Obviously, this is due to the occurrence and development of the porous skin at the fiber surface, the mechanical properties of which being very poor. Conversely, Fig. 20(b) shows that the elastic modulus values are not affected in the same temperature range, but later. In fact, testing fibers with such a porous skin equals testing fibers with smaller diameters. This affects the ultimate tensile strength value but not the modulus. The sudden decrease in the modulus value (Fig. 20(b)) from T_p = 1400–1450°C can be related to the overall SiC crystallization. This does not match with the behavior of the Si–C–O-based fiber from this work[27] or the Nicalon fiber,[16] for which the decrease in modulus is rather related to the intergranular phase degradation. This can be explained by the fact that the SiC crystallization follows the $SiO_xC_yN_z$ intergranular phase degradation in the former, while it occurs prior to the SiO_xC_y intergranular phase degradation in the latter. As far as crystals are linked one to each other through the intergranular phase, both moduli are able to be added.[16] As soon as they are dispersed in a surrounding phase being degraded, they act as heterogeneities prejudicial to the stiffness of the material.

5 Conclusion

The study has shown what were the similarities and the discrepancies between nitrogen-free and nitrogen-containing ceramics, with regard to their respective thermal behavior. As for any ceramic material taken within the Si–C–N–O system, carbon BSUs nucleate first. The chemical degradation is led by the thermostability of the amorphous continuum (intergranular) phase and controlled by the gas diffusion. Obviously, nitrogen—particularly when added to oxygen—is able to improve the thermostability of this phase and also to delay the SiC crystal nucleation by hindering the structural rearrangements. Consequences are that weight loss is prevented for a while and that mechanical properties of Si–C–N–O fibers are maintained longer than for mere Si–C–O fibers. The basic difference between the Si–C–N–O system compared to the ternary systems (Si–C–O, Si–C–N) is that the SiC crystal nucleation and the subsequent grain growth are delayed enough to occur at high temperature, after the beginning of the thermochemical degradation of the continuum. This induces a specific mechanism of grain growth. Using a nitrogen atmosphere helps to demonstrate that N_2 is one of the main gaseous species involved in the degradation mechanism.

Acknowledgements

The authors thank the national program Précurseurs de céramiques à base Si, C, N, O for its financial support and specifically the Centre National de la Recherche Scientifique (CNRS), the French Ministry of Defence (DRET), Rhône-Poulenc and Société Européenne de Propulsion. They also thank Mrs Kihn (Laboratoire d'Optique Electronique de Toulouse) for help in EELS measurements, and Mrs Oberlin for fruitful discussion.

References

1. Penn, B., Ledbetter, F. E., Clemons, J. M. & Daniels, J. G., Preparation of silicon carbide–silicon nitride fibers by the controlled pyrolysis of polycarbosilazane precursors. *J. Appl. Polym. Sci.*, **27** (1982) 3751–61.
2. Gaul, Jr, J. H., Process for the preparation of poly (disilyl)silazane polymers and the polymers therefrom. US Patent 4 340 619, 1982.
3. Cannady, J. P., US Patent 4 535 007, 1985.
4. Bacqué, E., Dunoguès, J., Biran, C., Olry, P. & Pillot, J. P., *French Patent* 2 599 037, 1986.
5. Laine, R. M., Blum, Y. D., Chow, A. & Schwartz, K. S., Silicon nitride ceramic fibers from preceramic polymers. Office of Naval Research (USA), *Techn. Rep.*, **8** (1987).
6. Isoda, T., Kaya, H., Arai, M., Nishi, H., Funuyama, O., Tashito, Y., Suzuki, T. Aoki, H., Ichiyama, M., Kato, T., Koshi, I. & Sato, K., In *SAMPE 89 Proceedings*. Japan, 1989, p. 912.
7. Caix, O. & Perez, G., Fiberamic^R: a new silicon carbonitride ceramic fiber with high therma stability. In *SAMPE 90 Proceedings*. Anaheim, USA, 1990, pp. 1–8.
8. Lavedrine, A., Bahloul, D., Goursat, P., Choong, K. Y. N., Corriu, R., Leclerc, D., Mutin, H. & Vious, A., *J. Eur. Ceram. Soc.*, **8** (1991) 221–7.
9. Richard, C., Bacqué, E., Pillot, J. P., Birot, M., Dunoguès, J., Mocaer, D. & Pailler, R., In *Actes Journées Spéciales Fibres Minérales*. Paris, France, 1991, pp. 7–16.
10. Delverdier, O., Monthioux, M., Mocaer, D. & Pailler, R., Thermal behavior of polymer-derived ceramics. III. Si–C–N system from a new PCSZ precursor. In *5th European Conference on Composite Materials Proceedings*, ed. A. R. Bunsell, J. F. Jamet & A. Massiah. Bordeaux, France, 1992, pp. 691–6.
11. Monthioux, M., Oberlin, A. & Bouillon, E., Relations between microtexture and electrical properties during heat-treatment of SiC fiber precursor. *Compos. Sci. Technol.*, **37** (1990) 21–35.
12. Delverdier, O., Monthioux, M., Oberlin, A., Lavedrine, A., Bahloul, D. & Goursat, P., Thermal behavior of polymer-derived ceramics. II. Si–C–N system from a new PVSZ precursor. *J. High Temp. Chem. Process.*, **1** (1992) 39–49.
13. Delverdier, O., Monthioux, M., Mocaer, D. & Pailler, R., Thermal behavior of polymer-derived ceramics. I. Si–C and Si–C–O systems from PCS precursors. *J. Eur. Ceram. Soc.*, **12** (1993) 27–41.
14. Mocaer, D., Pailler, R., Naslain, R., Richard, C., Pillot, J. P. & Dunoguès, J., Si–C–N ceramics with a high microstructural stability elaborated from the pyrolysis of new polycarbosilazane precursors. Part I. The organic–inorganic transition. *J. Mater. Sci.*, **28** (1993) 2615–31.
15. Mocaer, D., Pailler, R., Naslain, R., Richard, C., Pillot, J. P., Dunoguès, J., Delverdier, O. & Monthioux, M., Si–C–N ceramics with a high microstructural stability elaborated from the pyrolysis of new polycarbosilazane precursors. Part III. Effect of pyrolysis conditions on the nature and properties of oxygen-cured derived monofilaments. *J. Mater. Sci.*, **28** (1993) 2639–53.
16. Le Coustumer, P., Monthioux, M. & Oberlin, A., Understanding Nicalon^R fiber. *J. Eur. Ceram. Soc.*, **11** (1993) 95–103.
17. Le Coustumer, P., Etude du système Si–O–C. Exemple de la fibre Nicalon série 200. PhD Thesis, University of Pau & Pays de l'Adour, France, 1991.
18. Sawyer, L. C., Chen, R. T., Haimbach IV, F., Harget, P. J., Prack, E. R. & Jaffe, M., Thermal stability characterization of SiC ceramic fibers: II. Fractography and structure. *Ceram. Eng. Sci. Proc.*, **7** (1986) 914–29.
19. Lipowitz, J., Freeman, H. A., Chen, R. T. & Prack, E. R., Composition and structure of ceramic fibers prepared from polymer precursors. *Adv. Ceram. Mater.*, **2** (1987) 121–8.
20. Portre, L. & Sartre, A., Evidence for a silicon oxycarbide phase in the Nicalon silicon carbide fibre. *J. Mater. Sci.*, **24** (1989) 271–86.
21. Laffon, C., Flanck, A. M., Lagarde, P., Laridjani, M., Hagège, R., Olry, P., Cotteret, J., Dixmier, J., Miquel, J. L., Hommel, H. & Legrand, A. P., Study of Nicalon-based ceramic fibres and powders by EXAFS spectrometry, X-ray diffractometry and some additional methods. *J. Mater. Sci.*, **24** (1989) 271–86.
22. Huttepain, M. & Oberlin, A., Microtexture of non-graphitizing carbons and TEM studies of some activated samples. *Carbon*, **28** (1990) 103–11.
23. Mah, T., Hecht, N. L., McCulleim, D. E., Hoenigman, J. R., Kim, H. M., Katz, A. P. & Lipsitt, H. A., Thermal

stability of SiC fibres (Nicalon^{R}). *J. Mater. Sci.*, **19** (1984) 1191–201.
24. Durham, S. J. P., Shanker, K. & Drew, R. A. L., Carbothermal synthesis of silicon nitride: Effect of reaction conditions. *J. Amer. Ceram. Soc.*, **74** (1991) 31–7.
25. Filsinger, D. H. & Bourrie, D. B., Silica to silicon: Key carbothermic reactions and kinetics. *J. Amer. Ceram. Soc.*, **73** (1990) 1726–32.
26. Riley, F. J., *Progress in Nitrogen Ceramics.* Nijhoff, 1983, pp. 23–42.
27. Bouillon, E., Mocaer, E., Villeneuve, J. F., Pailler, R., Naslain, R., Monthioux, M., Oberlin, A., Guimon, C. & Pfister, G., Composition–microstructure–property relationships in ceramic monofilaments resulting from the pyrolysis of a polycarbosilane precursor at 800 to 1400°C. *J. Mater. Sci.*, **26** (1991) 1517–30.